ELSEVIER

Journal of Nuclear Materials 289 (2001) 1–9

journal of nuclear materials

www.elsevier.nl/locate/jnucmat

Section 1. Fabrication and properties of SiC composites and other ceramics

Tensile strength and fracture surface characterization of Hi-Nicalon™ SiC fibers

G.E. Youngblood [a,*], Charles Lewinsohn [a], R.H. Jones [a], Akira Kohyama [b]

[a] *Pacific Northwest National Laboratory, MS K2-44, P.O. Box 999, Richland, WA 99352, USA* [1]
[b] *Institute of Advanced Energy, Kyoto University, Kyoto, Japan*

Abstract

Dimensional, tensile strength and fracture surface characterizations were carried out for a particular batch of Hi-Nicalon™ SiC fiber. In general, filaments with larger cross-sectional areas (equivalent diameters) had lower strengths than filaments with smaller cross-sectional areas. A cyclic variation of fiber diameter along filament lengths was discovered with a repeat distance of about 16-cm and a maximum rate of change of about ± 0.6 μm/cm. During tensile tests at room temperature, fracture originated at critical flaws that typically consisted of internal pores or carbonaceous inclusions. Well-demarcated mirror and hackle regions usually surrounded the critical flaws. With a few exceptions, the critical flaw size (a_c) was linearly related to the mirror size (r_m) by $a_c \approx 0.33 r_m$. From fracture mechanics principles, values for the average mirror constant (A_m) and effective fracture toughness for this batch of Hi-Nicalon™ fiber were estimated to be 2.99 ± 0.33 and 1.1 ± 0.2 MPa $m^{1/2}$, respectively.

PACS: 62.20.Mk; 81.05.Mh; 81.70.B+; 81.05.Lg

1. Introduction

For several years, silicon carbide (SiC) composites consisting of a SiC matrix reinforced with continuous SiC fiber (SiC_f/SiC) have been examined for potential applications as a structural material in several fusion reactor concepts [1]. The performance of SiC_f/SiC, especially its toughness and high ultimate strength, depends upon the effectiveness of the interphase component and the high strength of the fiber component [2]. Therefore, in a neutron radiation environment the selected SiC fiber component, in particular, must exhibit strength retention as well as dimensional stability. In initial experiments, irradiated SiC fibers made with near-stoichiometric, crystalline SiC fibers exhibited the least property degradation [3,4]. Therefore, an extensive program to further examine the radiation performance of several types of advanced fibers with near-stoichiometric SiC compositions (Hi-Nicalon™, Hi-Nicalon™ Type S, Tyranno™ SA and Dow Sylramic™ fibers), has been initiated [5]. These fiber types are polymer-derived with small diameters and are suitable for weaving into fabric for SiC_f/SiC composite reinforcement.

The latter three fiber types listed above have SiC compositions with C/Si < 1.05 atomic, but only recently have they become available in limited quantities. On the other hand, the Hi-Nicalon™ fiber, which contains excess carbon (C/Si = 1.39 atomic), has been commercially available and used for SiC_f/SiC fabrication for several years. Furthermore, sufficient data have been obtained for the Hi-Nicalon™ fiber and composites made with this fiber that it now represents a standard for comparison of radiation effects [6]. Therefore, in this study the Hi-Nicalon™ fiber was selected to establish a base line for assessing the radiation performance of the other selected SiC fiber types. This report examines in detail the dimensional and strength characteristics for a particular batch of unirradiated Hi-Nicalon™ fiber (batch J2) to establish a base line as well as a test protocol for later irradiation performance evaluations.

* Corresponding author. Tel.: +1-509 375 2314; fax: +1-509 375 2186.
E-mail address: ge.youngblood@pnl.gov (G.E. Youngblood).

[1] Operated for the US DOE by Battelle Memorial Institute under Contract De-AC06-76RLO 1830.

0022-3115/01/$ - see front matter
PII: S0022-3115(00)00675-9

2. Experimental procedures

A detailed dimensional, tensile strength and fracture surface analysis was performed on the unirradiated batch J2 Hi-Nicalon™ SiC fiber. Batch J2 consisted of two short tow lengths cut from a 100 m spool labeled lot #225103, which was received in 1995 from the Nippon Carbon, Yokohama, Japan. The radiation stability of the Hi-Nicalon™ fiber, as well as the other selected SiC fiber types, will be assessed by repeating these analyses and comparing the induced changes after irradiation [4]. The planned irradiation will be carried out in the HFIR reactor at 300, 500 and 800°C to a dose of ≈10 dpa-SiC [5]. The post-irradiation testing should be completed by mid-2001.

Initially, filament diameter (cross-sectional shape) variations across and along a tow were examined for each of the four advanced SiC fiber types. The typical diameter variation across a tow was determined by SEM examination of approximately 500 filament cross-sections for a mounted and polished tow. An image analysis method, described in detail elsewhere [6], was used. To investigate the typical fiber diameter variation along filament lengths, three neighboring 0.25-m long filaments were pulled from a tow and cut sequentially into 25 segments, each 0.01-m long. Soaking the fiber tows in boiling water for ≈30 min and pulling the single filaments while still wet aided the filament separation. The mean segment diameter was determined from measurements of the maximum and minimum diameters made directly from an SEM image of the end of each segment viewed normal to its length. The ends of each segment were carefully retained in register so that the diameters represented the variation of the diameter along the filament length at 0.01-m intervals.

Sixty (60) filaments were selected at random from the Hi-Nicalon™ batch J2 and cut into 50 mm-lengths. Similar 50-mm length fiber bundles also are currently being irradiated. Tensile tests were carried out on this set of 60 filaments at ambient conditions using a Micropull™ Tensile Machine equipped with a 90 Newton load cell (Micropull Science, Thousand Oaks, CA). The tensile tests generally followed ASTM-recommended procedures [7], except filament diameters determined for the surface containing the fracture origin were used to calculate fracture stresses rather than using a nominal or average filament diameter. To do this, each 50-mm filament length was mounted by centering and fastening its ends with quick-setting cyanoacrylate glue (Loctite 404 Quick Set™, Hartford, CT) onto a split cardboard frame with a 25.4-mm window that defined the filament gauge length (Fig. 1). Load was applied at a constant displacement rate of 0.3 mm/min, which for uniform strain was equivalent to a strain rate of 2.2×10^{-4} s^{-1}. The filament breaking forces were between 0.2 and 0.8 N. However, the stored energy density was high (about 25 MJ/m^3). The sudden release of this stored elastic energy at fiber fracture caused the test filaments to fracture into multiple small segments due to the induced shock wave. Therefore, a procedure to dampen the shock wave and to capture the broken filaments was developed. The developed procedure was designed to be simple enough to be carried out inside a fume hood for later tensile testing of irradiated fibers.

A small rectangular plate (6.0×38 mm^2) was cut from a glass microscope slide and coated on one side with glycerin from an eye dropper. The plate was carefully bridged across the cardboard mounting frame (Fig. 1) so that the filament to be tested was completely wetted by glycerin. By this mounting arrangement, the filament did not support the weight of the glycerin anywhere along its gauge length because the glycerin was held by surface tension to the under-side of the glass plate. The glycerin effectively damped the shock wave in the filament and it usually fractured only at one location [8]. Each fiber segment remained attached to its half of the mounting frame which is important for later easy recovery and disposal of irradiated fibers.

To examine the individual filament segments, the following technique was adopted. The fracture location was first noted. Fracture of the filament at the edge of the window frame might mean that a bending moment caused the fracture. Only a few filaments fractured at the edge of the mounting frame, so these tests were discarded. Each filament segment for the successful tests was gripped with blunt-nosed tweezers and broken off at the frame edge. While retaining the grip, the glycerin adhered to each segment was removed by careful agitation in isopropyl alcohol for about 30 s. The segments

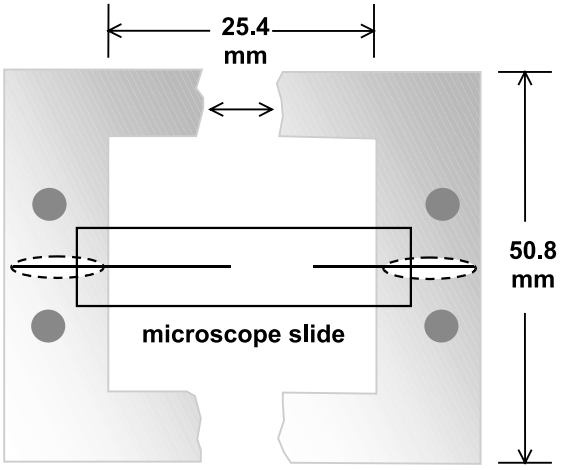

Fig. 1. Schematic drawing of fiber mounting showing a pair of fractured segments retained in thin glycerin strip deposited on bottom side of the bridging 6.0×38 mm^2 glass microscope slide.

were mounted on two-sided carbon tape applied to the cut face of an aluminum SEM mounting disc cut in half. Usually about 10 segments were mounted per half-disc face with each pair of matching filament fracture surfaces aligned and protruding ≈1 mm above the disc surface. The other half-disc was stuck to the carbon tape to reform a full disc and secure all the mounted fiber segments along the disc diameter. Then, the fracture surfaces of the aligned filaments could easily be located, identified and imaged by SEM.

The equivalent diameter of the actual fracture surface was determined by measuring the maximum and minimum diameters from each SEM image with a caliper and averaging the measurements taken from each of the mating segments. Other fracture surface features (critical flaw size, type and location and the surrounding mirror, mist and hackle) also were identified and measured. The flaw and mirror sizes were taken as the largest defined dimension across a feature. A normalized flaw location (λ) was defined as the distance from the center of the filament to the center of the flaw divided by the filament radius measured along the same line. Thus, $\lambda = 1$ for a flaw at the filament surface; $\lambda = 0$ for a flaw at the filament center, etc.

Weibull strength and strength distribution analysis (two-parameter) and a systematic fracture surface analysis were then carried out for a data set obtained for 51/60 unirradiated and successfully tested Hi-Nicalon™ (batch J2) filament pairs according to ASTM C1239-95 procedures [9].

3. Results

The typical diameter variation across a tow for Hi-Nicalon™ fiber, as determined by the image analysis method, ranged from 7 to 20 μm with an average diameter of 13.8 μm, and exhibited a near normal distribution with a 1σ standard deviation of ±13% [6]. Fiber diameter variations along three neighboring 0.25-m filaments selected from batch J2 are displayed in Fig. 2. The diameter typically varied by 1.5–2.5 μm over the 0.25-m lengths. Interestingly, each filament displayed an in-register cyclic variation with a repeat distance of ≈0.16 m and a maximum rate of change of about ±0.6 μm/cm.

Other characterization measurements for this particular batch of Hi-Nicalon™ fiber, including bulk density, electrical resistivity, thermal conductivity, and crystallite size determinations by XRD, were made and reported previously [4]. Several of the measured lot specific properties are compared to nominal Hi-Nicalon properties in Table 1.

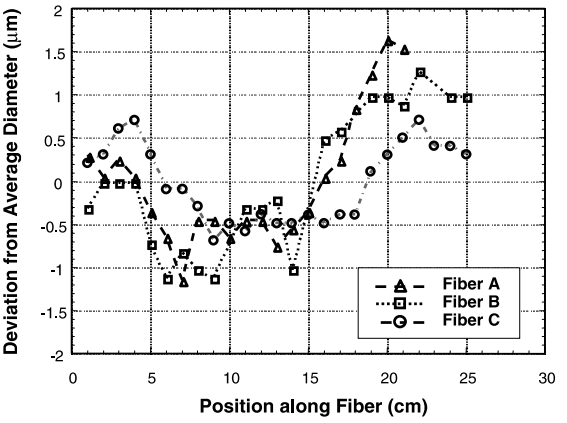

Fig. 2. Fiber diameter variation along the lengths of three neighboring 0.25-m filaments.

Table 1
Comparison of nominal with measured batch specific properties for Hi-Nicalon™ SiC fiber

Property	Reference[a]	PNNL[b]
Diameter (μm)	14	13.8 ± 1.8
Bulk density (g/cm^3)	2.74	2.69 ± 0.01
Tensile strength (GPa)	2.8	2.59 ± 0.51
Tensile modulus (GPa)	270	–
Electric resistivity (Ω-cm)	1.4	3.0 ± 0.2
Specific heat (J/gK)	0.67 at 25°C	0.68 at 25°C
	1.17 at 500°C	1.17 at 500°C
Thermal conductivity (W/mK)	7.8 at 25°C	5.05 at 25°C
	10.1 at 500°C	6.30 at 500°C
C/Si (atomic)	1.39	–
Oxygen content (wt%)	<0.5	–
XRD grain size (nm)	4	4.0 ± 0.3
Fracture toughness (MPa m$^{1/2}$)	–	1.1 ± 0.6

[a] Nippon Carbon, Eng. and Sci. Proc. 19(3), 55, 1998.
[b] Batch #225103(6/27/95).

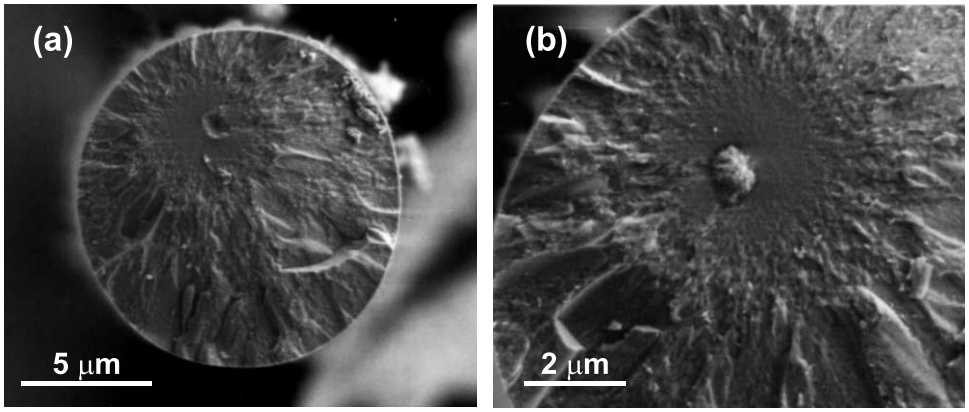

Fig. 3. An SEM of a typical pair of mating fracture surfaces showing in: (a) an internal pore and the surrounding mirror and hackle regions, and in (b) the actual critical flaw was an inclusion that popped free from the opposite pore. For this sample, $d = 12.8$ μm, $S_f = 2.89$ GPa, $\lambda = 0.44$, $r_m = 1.34$ μm and $a_c = 0.61$ μm.

Typical fracture surface features observed for the unirradiated batch J2 Hi-Nicalon™ fiber are illustrated in the following SEM micrographs. In Fig. 3(a) and (b), a mating pair of fracture surfaces shows a critical flaw and the surrounding mirror, mist and hackle regions typical of brittle fracture. The pore in (a) matches the nodular inclusion in (b). For this particular filament, the equivalent diameter and the mirror and critical flaw radii were determined to be 12.8, 1.34 and 0.61 μm, respectively. The tensile strength (S_f) was 2.89 GPa, and the normalized flaw location (λ) was 0.44.

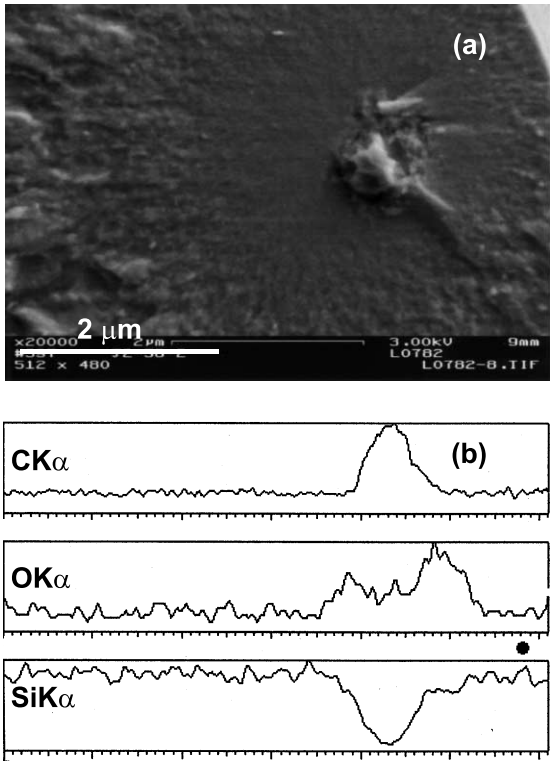

Fig. 4. An enlarged SEM view of: (a) an inclusion-type critical flaw and (b) the corresponding C, O and Si EDS line scans across the inclusion. For this sample, $d = 13.1$ μm, $S_f = 2.23$ GPa, $\lambda = 0.70$, $r_m = 1.41$ μm and $a_c = 0.46$ μm.

In Fig. 4(a) and (b), a higher magnification of a typical inclusion is shown in (a) while several EDS line scans taken across the inclusion and the surrounding region are shown in (b). The pertinent dimensional and strength data for this particular filament are given in the figure caption. The three line scans qualitatively show the variation of the C, O and Si concentrations in the region of the critical flaw. The relative concentrations of C, O and Si are constant until the inclusion is encountered by the scan, where the C concentration abruptly increases and the Si concentration abruptly decreases at the edge of the inclusion. The O concentration appears to increase above its base-line level (which should be quite low in Hi-Nicalon) just prior to encountering the inclusion, drops slightly along the path across the inclusion, and increases again on the other side of the inclusion before dropping back to base-line levels. The inclusion (critical flaw) appears to be a region of unreacted carbon, probably a remnant from incomplete mixing of the polymer precursors used during fiber processing. Apparently, the oxygen shell surrounding the inclusion somehow played a role in preventing the proper mixing of Si and C components. Inclusion nodules with similar characteristics were observed in other fracture surface views as well.

Sometimes both sides of the mating fracture surface exhibited only a well-demarcated pore, as illustrated in Fig. 5(a) and (b). For this type of flaw, it is possible that

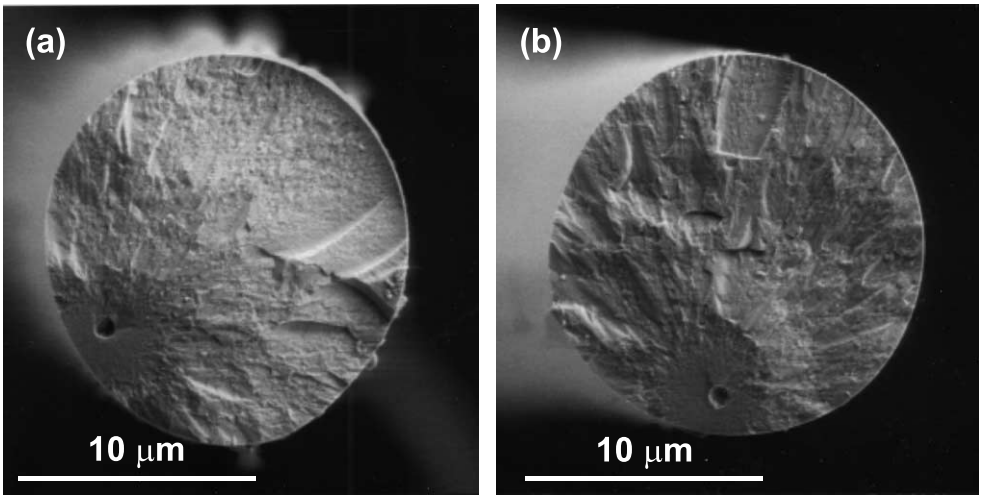

Fig. 5. (a) and (b) An SEM of a typical pair of mating fracture surfaces showing an internal pore (critical flaw) in each surface. For this sample, $d = 15.3$ μm, $S_f = 2.40$ GPa, $\lambda = 0.83$, $r_m = 1.23$ μm and $a_c = 0.45$ μm.

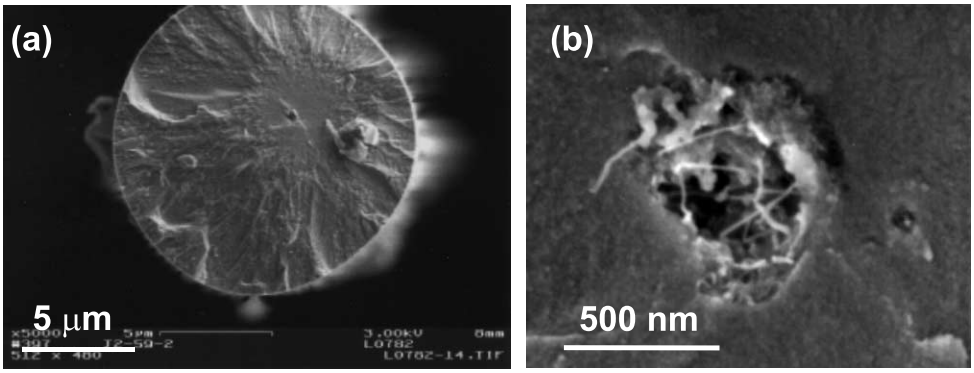

Fig. 6. An SEM of a pair of mating fracture surfaces showing in: (a) an internal pore (critical flaw), and in (b) delicate fibrils bridging the pore. For this sample, $d = 13.4$ μm, $S_f = 2.69$ GPa, $\lambda = 0.27$, $r_m = 1.21$ μm and $a_c = 0.39$ μm.

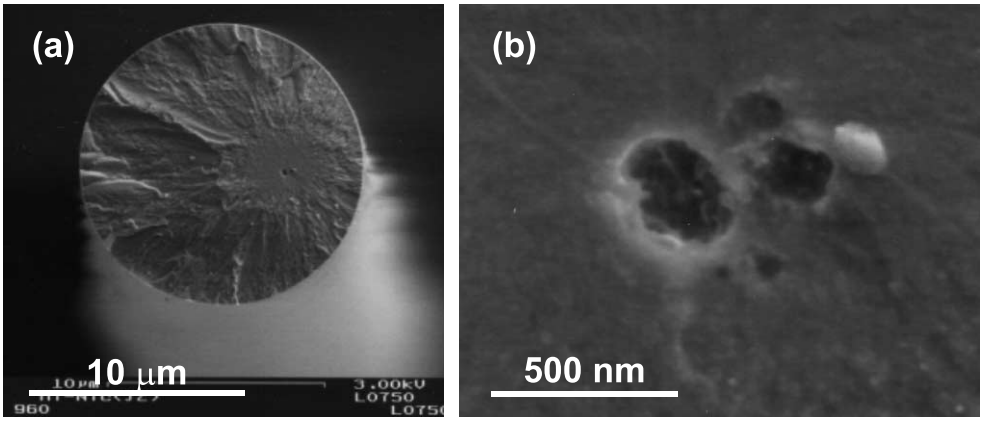

Fig. 7. An SEM of a pair of mating fracture surfaces showing in: (a) an internal pore (critical flaw), and in (b) an enlarged view of a multi-pore flaw. For this sample, $d = 13.0$ μm, $S_f = 3.00$ GPa, $\lambda = 0.48$, $r_m = 1.09$ μm and $a_c = 0.26$ μm.

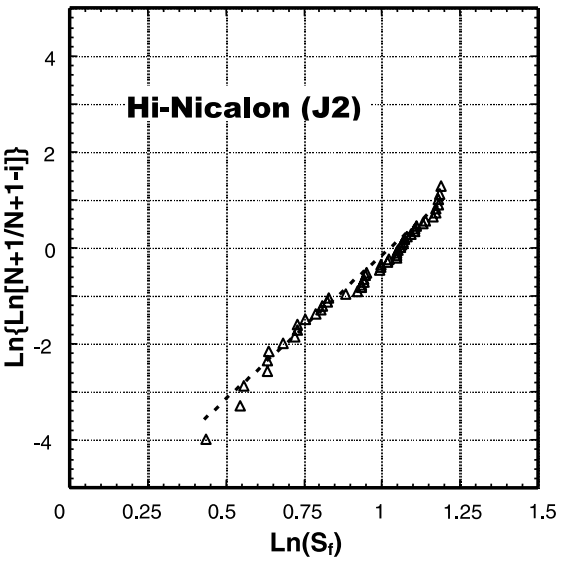

Fig. 8. A two-parameter Weibull plot for the 51 Hi-Nicalon (batch J2) tensile strength data points. The Weibull scale parameter and modulus values extracted from this plot were 2.79 and 5.99 GPa, respectively.

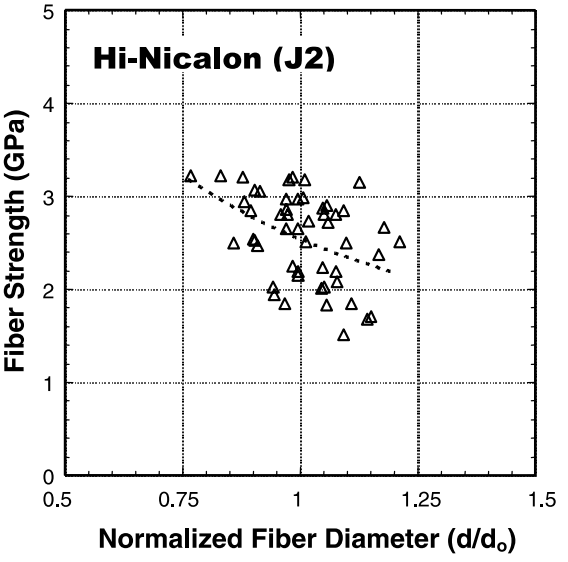

Fig. 9. The fiber tensile strength vs. the normalized diameter (Hi-Nicalon batch J2).

a carbon-type nodule actually popped free during the tensile fracture test leaving only the remaining pore from which it escaped. In Fig. 6(a) and (b), on the other hand, a fracture surface image shows an internal pore in (a) while an enlarged view in (b) shows delicate fibrils bridging the pore. Obviously, the fibril-bridged pore did not contain a nodule, but was gas-filled. Finally, in Fig. 7(a) and (b) a fracture surface image shows a relatively small internal flaw in (a), while an enlarged view in (b) reveals that the flaw actually consisted of several smaller pores. Again, the pertinent dimensional and strength data for each tested filament are given in the figure captions.

For the set of 51 filaments successfully tested, 62% of the critical flaws were identified as single or multiple pores with radii ranging from 0.1 to 1.1 μm. The other 38% were nodule or granular inclusions with similar dimensions.

In Fig. 8, a two-parameter Weibull plot showing the tensile strength distribution for the unirradiated Hi-Nicalon™ (batch J2) fiber is presented. From this plot, a Weibull scale factor $\sigma_0 = 2.79$ GPa and a modulus $\beta = 5.99$ were determined. The Weibull average strength (σ_{avg}) was calculated to be 2.59 ± 0.51 GPa from the relation $\sigma_{\text{avg}} = \sigma_0 \Gamma(1 + 1/\beta)$, where $\Gamma(1 + 1/\beta)$ is a gamma function value [10].

In Fig. 9, the fiber tensile strength dependence on the normalized filament diameter (determined by dividing the mean filament diameter for each fracture surface by the average filament diameter for the tested J2 fibers) is illustrated. Despite significant scatter, the general trend that fibers with larger diameters have lower strengths is noted.

In Fig. 10, the dependence of the critical flaw size on its corresponding mirror size is examined. Although there are a few noticeably large deviations, a straight line passing through the origin was used to fit the data by linear regression. The resultant slope of this line was 0.33.

In Fig. 11, the individual filament strengths are compared to the mirror sizes for the tested J2 fibers. The normalized mirror size (r_m/r_0) was determined by dividing each r_m-value by the average mirror radius (r_0),

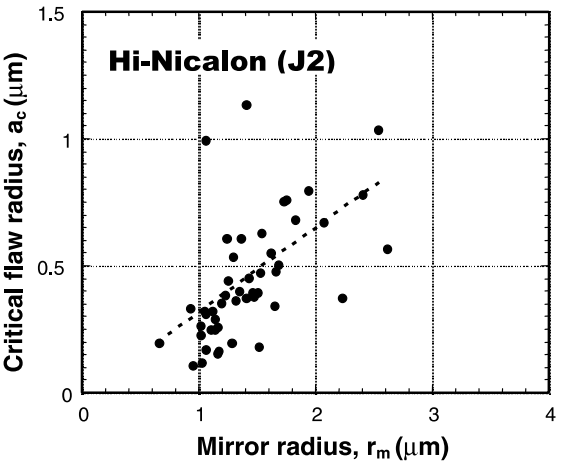

Fig. 10. The critical flaw radius vs. the mirror radius (Hi-Nicalon batch J2).

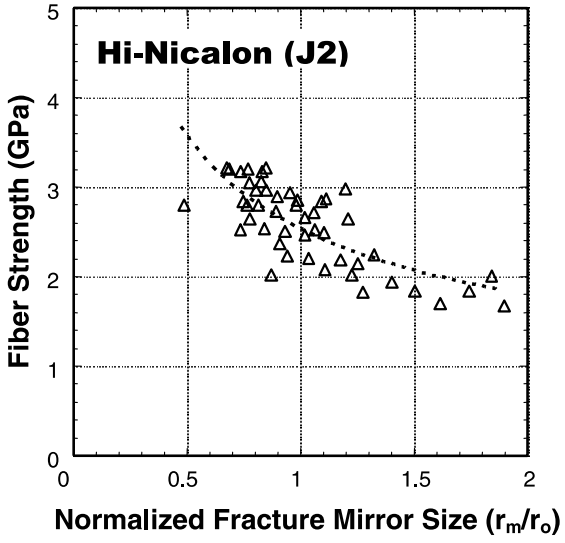

Fig. 11. The fiber tensile strength vs. the normalized mirror radius (Hi-Nicalon batch J2).

which was 1.41 μm for the tested filaments. The data were fit to a simple power law $S_f = S_0(r_m/r_0)^{-n}$. The result of a linear regression fit was $S_f = 2.54(r_m/1.406)^{-0.495}$ with a correlation coefficient $R = 0.73$.

In Fig. 12, a possible tensile strength dependence on critical flaw location is examined. The data exhibit quite a bit of scatter, but no apparent strength dependence on flaw location is evident. For the batch J2 fibers, the critical flaws rarely occurred at the filament surface, but mostly were distributed internally with only a slight preference for being located nearer to the filament surface than to the filament center. Also, when the flaw types were recorded alongside each data point, no dependence of the fiber strength on the flaw type (single or multiple pore or inclusion) was discerned. A similar plot (not given) indicated that flaw sizes also were independent of their location for this data set.

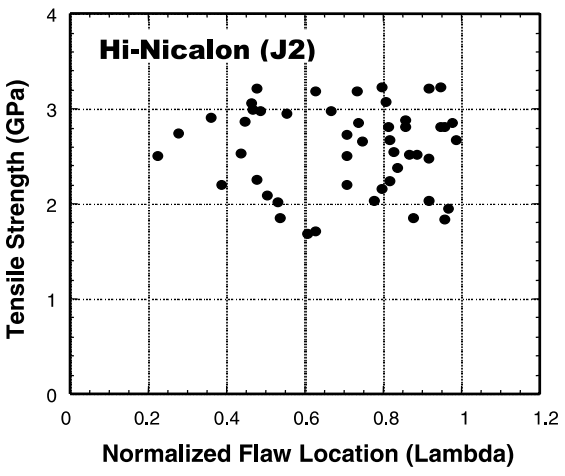

Fig. 12. The fiber tensile strength vs. the normalized flaw location (Hi-Nicalon batch J2).

4. Discussion

Because of the relatively wide filament diameter variations that occur across tows (7–20 μm) as well as along single filaments (1–2 μm/25.4 mm gauge length), for the batch J2 fibers, use of a nominal or batch average fiber diameter to determine individual filament strengths is not appropriate. For instance, a 10% error in diameter would result in about a 20% error in the calculated breaking stress. Such errors cause additional scatter in the Weibull strength distribution, which results in smaller values of β. In such cases, to properly assess the fiber strength and its distribution, the fiber cross-sectional area (equivalent diameter) determined for the fracture surface should be used to calculate the fracture stress. This is the likely situation for most polymer-derived SiC fibers that are processed using a spinning method [11].

Two types of critical flaws (pores and inclusions) were observed for the batch J2 Hi-Nicalon™ fibers. Since both types of critical flaws appeared to have similar sizes and size distributions, they were assumed to represent a single type of flaw population. A simple two-parameter Weibull analysis should be appropriate to assess the tensile strength and strength distribution for such a batch of fibers. Generally, radiation-induced flaws in SiC fibers have a quite different appearance and occur at the fiber surface [12]. A simple Weibull analysis may not be appropriate when two distinctly different types of flaws with different flaw distributions occur [13].

The average tensile strength of the J2 batch of Hi-Nicalon™ (2.59 ± 0.51 GPa) was somewhat lower than the manufacturer's listed value of 2.8 GPa (Table 1). All of the critical flaws were internal and many of them consisted of fairly large carbonaceous inclusions, which suggest that the flaws resulted because of processing conditions, not handling. For these reasons, it is likely that the J2 batch of Hi-Nicalon™ was slightly substandard compared to normally available stock. The slightly lower than nominal bulk density and thermal conductivity values noted in Table 1 for this batch of Hi-Nicalon™ support this suggestion.

The significant scatter noted in the tensile strength-fiber diameter data for the J2 batch of Hi-Nicalon™ fibers (Fig. 9) is due to the wide range of internal critical flaw sizes. The trend that filaments with larger diameters are weaker was reported previously for the Hi-Nicalon™ fiber [6] as well as for other polymer-derived SiC fibers [11]. A three-parameter Weibull analysis, as suggested by Zhu et al. [15] may be more appropriate to accurately

describe the strength and strength distribution when the tested fibers exhibit such a strength dependence on filament diameter. However, the main goal for this analysis is to assess degradation of the fiber strength due to radiation effects, so the simpler two-parameter Weibull analysis will continue to be used.

A linear relationship between the critical flaw size (effective radius a_c) and the mirror size (radius r_m) is commonly observed for brittle fracture of glass or fine, polycrystalline materials [16]. The ratio $a_c/r_m = 0.33$ was somewhat larger than the 0.19–0.22 range of values observed for ceramic grade (CG) Nicalon fiber [11]. Some of the larger deviations from the linear relationship must be associated with the difficulty in estimating the actual flaw sizes from the SEM micrographs. Many of the flaw foot-prints were irregularly shaped. Rarely did they appear circular. However, in most cases the mirror regions surrounding the critical flaws appeared to have formed an approximately circular pattern. Therefore, the easier to measure r_m-value and the relation $a_c = 0.33r_m$, which averaged out individual discrepancies in determining the critical flaw size, was used for further analysis.

Again in Fig. 11, because of the Weibull statistics there was significant scatter in the power law fit to the S_f vs. (r_m/r_0) data. Nevertheless, the parameter $S_0 = 2.54$ GPa closely matches the Weibull average strength of 2.59 GPa (Table 1). The exponent $n = -0.495$ also is very close to the expected value of −0.5 for brittle fracture according to the Griffith theory [17].

Examination of Fig. 12 confirms that the tensile strengths for the batch J2 fiber did not depend upon critical flaw location, but primarily upon the critical flaw size. Taylor et al. [11] observed different flaw distributions for different flaw types (single pore, multi-pore or inclusions) for Nicalon™ CG fiber. However, such a difference was not apparent for our batch J2 data, possibly because there were insufficient data points. Nevertheless, such a difference would not be surprising for irradiated Hi-Nicalon™ or other irradiated SiC fiber types.

Fracture mechanics predicts a simple relation between flaw radius, fracture strength (S_f) and the critical fracture toughness (K_{1c}) for brittle materials [18].

$$S_f(a_c)^{1/2} = F(q)K_{1c} = \text{constant}. \quad (1)$$

In Eq. (1), $F(q)$ is a geometric factor dependent on the critical flaw shape and location and its relative size compared to the sample size. For a small, centrally located penny-shaped flaw in a plane normal to the tensile axis, $F(q) \approx 1.56$ [14]. Then, in principle, it is possible to estimate an effective fiber toughness from measurements of the filament strengths and mirror radii, since the critical flaw size is linearly related to the mirror size and the expected power dependence of −0.5 is approximately obeyed. Importantly, in an SEM view of a fracture surface the fracture mirror radius generally is easier to determine than the critical flaw radius.

Substituting $a_c = 0.33r_m$ and $F(q) = 1.56$ into Eq. (1) and rearranging terms, one gets

$$S_f = A_m(r_m)^{-0.5}, \quad (2)$$

where

$$A_m = F(q)(K_{1c})/(0.33)^{0.5} \approx 2.72(K_{1c}) \quad (3)$$

for the batch J2 Hi-Nicalon™ fibers.

In Fig. 13, the Hi-Nicalon (batch J2) fiber tensile strength data vs. $(r_m)^{-0.5}$ are plotted. The data were fit to a linear relation by regression analysis. The mirror constant (A_m), defined as the slope of the linear fit to the data and through the origin, was determined to be 2.99 ± 0.33 MPa $m^{1/2}$; and from Eq. (3) $K_{1c} = 1.1 \pm 0.2$ MPa $m^{1/2}$. The mirror constant was similar to the value (2.51 MPa $m^{1/2}$) reported for Nicalon CG fiber by Zhu and coworkers [11], but somewhat lower than the value (4.0 MPa $m^{1/2}$) reported for Hi-Nicalon fiber by Hurst et al. [19]. Since A_m is an average value, the K_{1c}-value determined for the J2 batch of Hi-Nicalon fibers also is an average value.

Hurst et al. reported a similar range of mirror and critical flaw sizes and a similar fraction of pore-type critical flaws (70%) for their batch of Hi-Nicalon™ fiber. However, they reported a fracture toughness value of 4–5 MPa $m^{1/2}$, which is considerably larger than the 1.1 MPa $m^{1/2}$ determined for our batch of fibers. This difference may be due to the fact that the balance of non-pore type critical flaws in our batch of fibers were carbonaceous inclusions, while the balance of non-pore type flaws in their batch of Hi-Nicalon fibers were surface anomalies. Apparently, the carbonaceous inclusion-type flaws were not observed by Hurst et al. The fairly

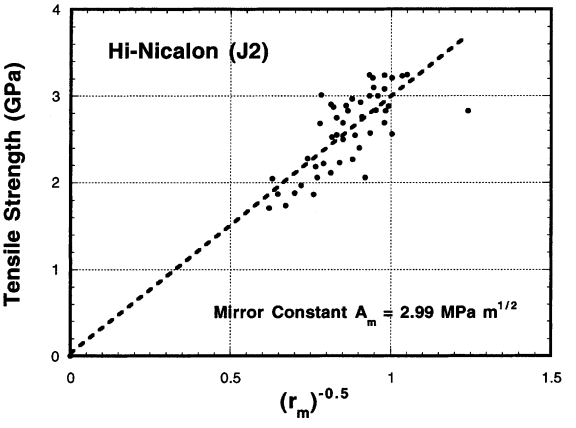

Fig. 13. The fiber tensile strength vs. the square root of the fracture mirror radius (Hi-Nicalon batch J2). The slope yields the mirror constant $A_m = 2.99 \pm 0.33$ MPa $m^{1/2}$.

large difference in fracture toughness values determined for these two different batches of Hi-Nicalon™ fibers suggests that the fiber fracture toughness is extremely sensitive to the fiber processing conditions.

Usually the critical mode-I fracture toughness K_{1c} values are determined by measuring the fast fracture strengths of bars with a machined flaw of well-defined dimensions and orientation [18]. Obviously the inherent critical flaws in the tensile-tested fibers do not fall into this category. Nevertheless, as this example for the tensile strength data set for a Hi-Nicalon™ fiber illustrates, effective fiber toughness values can be extracted from tensile test data by using fracture mechanics principles and fracture surface analysis if fracture mirrors are observable. The average fracture toughness value determined by the described method may be useful as a sensitive measure of the degradation effects due to irradiation for this batch of Hi-Nicalon™ fiber as well as for other SiC-type fibers.

5. Conclusions

A dimensional, tensile strength and fracture surface characterization protocol was established by analyzing in detail a particular batch of unirradiated Hi-Nicalon™ SiC fiber. In general, the filaments within a tow of Hi-Nicalon fiber exhibited a wide variation of diameters across the tow and along filament lengths. The filaments with larger cross-sectional areas (equivalent diameters) had lower strengths than filaments with smaller cross-sectional areas. For this batch of Hi-Nicalon™ fiber, a cyclic variation of fiber diameter along filament lengths was discovered with a repeat distance of about 0.16-m and a maximum rate of change of about ± 0.6 μm/cm. During tensile tests of the batch J2 Hi-Nicalon™ fibers at ambient conditions, fracture originated at critical flaws that typically consisted of internal pores or carbonaceous inclusions, which likely were introduced during processing. Well-demarcated mirror and hackle regions usually surrounded the critical flaws. With a few exceptions, the critical flaw size (a_c) was linearly related to the mirror size (r_m) by $a_c \approx 0.33 r_m$. The tensile strength depended primarily on the critical flaw size and not the flaw location or type. From fracture mechanics principles, an average mirror constant and an effective fiber toughness for the Hi-Nicalon™ (batch J2) fibers were estimated to have values of 2.99 ± 0.33 and 1.1 ± 0.2 Mpa $m^{1/2}$, respectively. The physical properties for the tested batch of Hi-Nicalon™ fiber were substandard compared to the nominal property values for Hi-Nicalon™ fiber, possibly due to the presence of numerous carbonaceous inclusions in the tested batch. Nevertheless, the test protocol should be appropriate for characterizing other advanced, polymer-derived SiC-type fibers and for assessing degradation in these fibers due to neutron irradiation.

Acknowledgements

The Fusion Energy Sciences Program of the US Department of Energy and the Monbusho Fusion Energy Program of Japan sponsored this collaborative research program.

References

[1] P. Fenici, A.J. Frias Rebelo, R.H. Jones, A. Kohyama, L.L. Snead, J. Nucl. Mater. 258–263 (1998) 215.
[2] W.A. Curtin, J. Am. Ceram. Soc. 74 (11) (1991) 2837.
[3] M.C. Osborne, C.R. Hubbard, L.L. Snead, D. Steiner, J. Nucl. Mater. 253 (1998) 67.
[4] G.E. Youngblood, R.H. Jones, A. Kohyama, L.L. Snead, J. Nucl. Mater. 258–263 (1998) 1551.
[5] G.E. Youngblood, R.H. Jones, A. Kohyama, Y. Katoh, A. Hasegawa, R. Scholz, L.L. Snead, in: Fusion Materials Semiannual Progress Report DOE/ER-0313/24, 1998, p. 115.
[6] G.E. Youngblood, R.H. Jones, A. Hasegawa, in: R.H. Jones, A. Kohyama (Eds.), Proceedings of the Third IEA Workshop on SiC/SiC Ceramic Composites for Fusion Structural Applications, Cocoa Beach, FL, 1999, p. 152.
[7] Standard D3379-75 (Reapproved 1989), American Society for Testing and Materials, West Conshocken, PA, 1989.
[8] L.C. Sawyer, M. Jamieson, D. Brikowski, M.I. Haider, R.T. Chen, J. Am. Ceram. Soc. 70 (11) (1987) 798.
[9] Standard C1239-95, American Society for Testing and Materials, West Conshocken, PA, 1995.
[10] S.N. Patankar, J. Mater. Sci. Lett. 10 (1991) 1176.
[11] S.T. Taylor, Y.T. Zhu, W.R. Blumenthal, M.G. Stout, D.P. Butt, T.C. Lowe, J. Mater. Sci. 33 (1998) 0000.
[12] G.E. Youngblood, unreported work.
[13] K. Gola, H. Fukunaga, J. Mater. Sci. 21 (1986) 4475.
[14] Y.T. Zhu, W.R. Blumenthal, S.T. Taylor, T.C. Lowe, J. Am. Ceram. Soc. 80 (6) (1997) 1447.
[15] Y.T. Zhu, S.T. Taylor, M.G. Stout, D.P. Butt, W.R. Blumenthal, T.C. Lowe, J. Mater. Sci. 33 (1998) 1.
[16] J.J. Mecholsky, R.W. Rice, S.W. Freiman, J. Am. Ceram. Soc. 57 (1974) 440.
[17] A.A. Griffith, Phil. Trans. Roy. Soc. A 221 (1920) 163.
[18] A.G. Evans, in: R.C. Brandt, D.P.H. Hasselman, F.F. Lange (Eds.), Fracture Mechanics of Ceramics, vol. I, Plenum Press, New York, 1974, p. 17.
[19] J. Hurst, H.-m. Yun, D. Gorican, in: N.P. Bansal, J.P. Singh (Eds.), Advances in Ceramic–Matrix Composites III, CT 74, 1996, p. 3.